npj | 2D Materials and Applications

www.nature.com/npj2dmaterials

ARTICLE OPEN

Check for updates

Noise diagnostics of graphene interconnects for atomic-scale electronics

László Pósa[1,2,5], Zoltán Balogh[1,3,5], Dávid Krisztián[1], Péter Balázs[1], Botond Sánta[1,3], Roman Furrer[4], Miklós Csontos[1,4] and András Halbritter[1,3]✉

Graphene nanogaps are considered as essential building blocks of two-dimensional electronic circuits, as they offer the possibility to interconnect a broad range of atomic-scale objects. Here we provide an insight into the microscopic processes taking place during the formation of graphene nanogaps through the detailed analysis of their low-frequency noise properties. Following the evolution of the noise level, we identify the fundamentally different regimes throughout the nanogap formation. By modeling the resistance and bias dependence of the noise, we resolve the major noise-generating processes: atomic-scale junction-width fluctuations in the nanojunction regime and sub-atomic gap-size fluctuations in the nanogap regime. As a milestone toward graphene-based atomic electronics, our results facilitate the automation of an optimized electrical breakdown protocol for high-yield graphene nanogap fabrication.

npj 2D Materials and Applications (2021)5:57 ; https://doi.org/10.1038/s41699-021-00237-w

INTRODUCTION

Recently discovered 2D materials have demonstrated their high potential[1] as the versatile components of flexible[2] or silicon-integrated two-dimensional electronic circuits.[3] Emerging applications include analog switches,[4–6] operational amplifiers,[7] flexible sensors,[8,9] or neuromorphic computing units.[10] Most of these device concepts exploit the complex electronic properties of transition metal dichalcogenide structures,[11] whereas graphene is utilized as an ideal two-dimensional conducting and contacting platform. Graphene nanogaps are widely considered as ideal circuit components to clamp a broad range of further nanoscale objects, such as single molecules or molecular assemblies,[12–15] DNA sequences,[16,17] or atomic-scale resistive switching filaments.[18–20] Thereby these structures can also be implemented as functional components of 2D circuits. The key aspects which make graphene an ideal contacting material are its single-atom thickness as well as its outstanding room temperature structural stability arising from the strong carbon-carbon bonds. Moreover, recently developed feedback-controlled electrical breakdown (EB) protocols[21–24] enabled the high-yield fabrication of graphene nanogaps and, thereby, the experimental realization of various, truly nanometer-sized graphene-nanostructure-graphene architectures.

However, the functional advantages of such ultra-small circuit elements are inevitably accompanied by the extreme challenges of imaging the relevant atomic-scale processes during their operation demanding cutting-edge microscopic techniques. Here we apply a fundamentally different approach by delivering such a microscopic insight through the analysis of the low-frequency noise characteristics. We demonstrate that the combined analysis of the noise's resistance and frequency dependence together with the application of nonlinear noise spectroscopy provide a rich source of information on the atomic-scale processes in graphene nanojunctions and nanogaps. In particular, we show that the evolution of the noise characteristics clearly indicate the transition between fundamentally different regimes of the nanogap formation process: in narrowing graphene junctions the rapidly increasing noise reflects truly atomic-scale junction-width fluctuations, whereas in the nanogap regime a saturated noise level arising from sub-atomic gap-size fluctuations is observed.

RESULTS AND DISCUSSION

Device preparation by gradual electrical breakdown

Our devices consist of bowtie-shaped CVD graphene sheets[25] terminated by two metal electrodes (see schematic in Fig. 1a). The constriction at the narrowest cross-section (Fig. 1b) is broken by a feedback-controlled electrobreakdown procedure in air at room temperature. The resulting nanometer-sized gap is visible as a dark gray line in the SEM image shown in Fig. 1c. Electrical breakdown is induced by periodically applied 200 µs long voltage pulses, whose amplitude (V_{Pulse}) is consecutively increased by 1 mV. Meanwhile the current (I_{Pulse}) is monitored (see Fig. 1d). To avoid the abrupt breakdown, we stop the voltage ramp when the current decreases by a certain percentage compared to the maximum current within the past 200 mV voltage interval (see Supplementary Note 1 for further details on this protocol). Repeating the voltage ramp cycles after each feedback event we can gradually increase the resistance until the desired nanogap is established. If the feedback event is not accompanied by a clear junction resistance increase, the threshold feedback percentage is increased in the next voltage ramp cycle.

To illustrate the gradual narrowing of the contact we plot the constriction resistance ($R_C = (V_{Bias}/I) - R_{Lead}$) as a function of the voltage ramp cycle number in Fig. 1e (see further examples for the evolution of R_C along the EB cycles in the Supporting Information). Since the initial resistance of the constriction is negligible, the lead resistance (R_{Lead}) is estimated by the lowest resistance value

[1]Department of Physics, Budapest University of Technology and Economics, Budafoki út 8, 1111 Budapest, Hungary. [2]Institute of Technical Physics and Materials Science, Centre for Energy Research, Konkoly-Thege M. út 29-33, 1121 Budapest, Hungary. [3]MTA-BME Condensed Matter Research Group, Budafoki út 8, 1111 Budapest, Hungary. [4]Empa, Swiss Federal Laboratories for Materials Science and Technology, Transport at Nanoscale Interfaces Laboratory, Überlandstrasse 129, CH-8600 Dübendorf, Switzerland. [5]These authors contributed equally: László Pósa, Zoltán Balogh. ✉email: halbritt@mail.bme.hu

Published in partnership with FCT NOVA with the support of E-MRS

npj nature partner journals

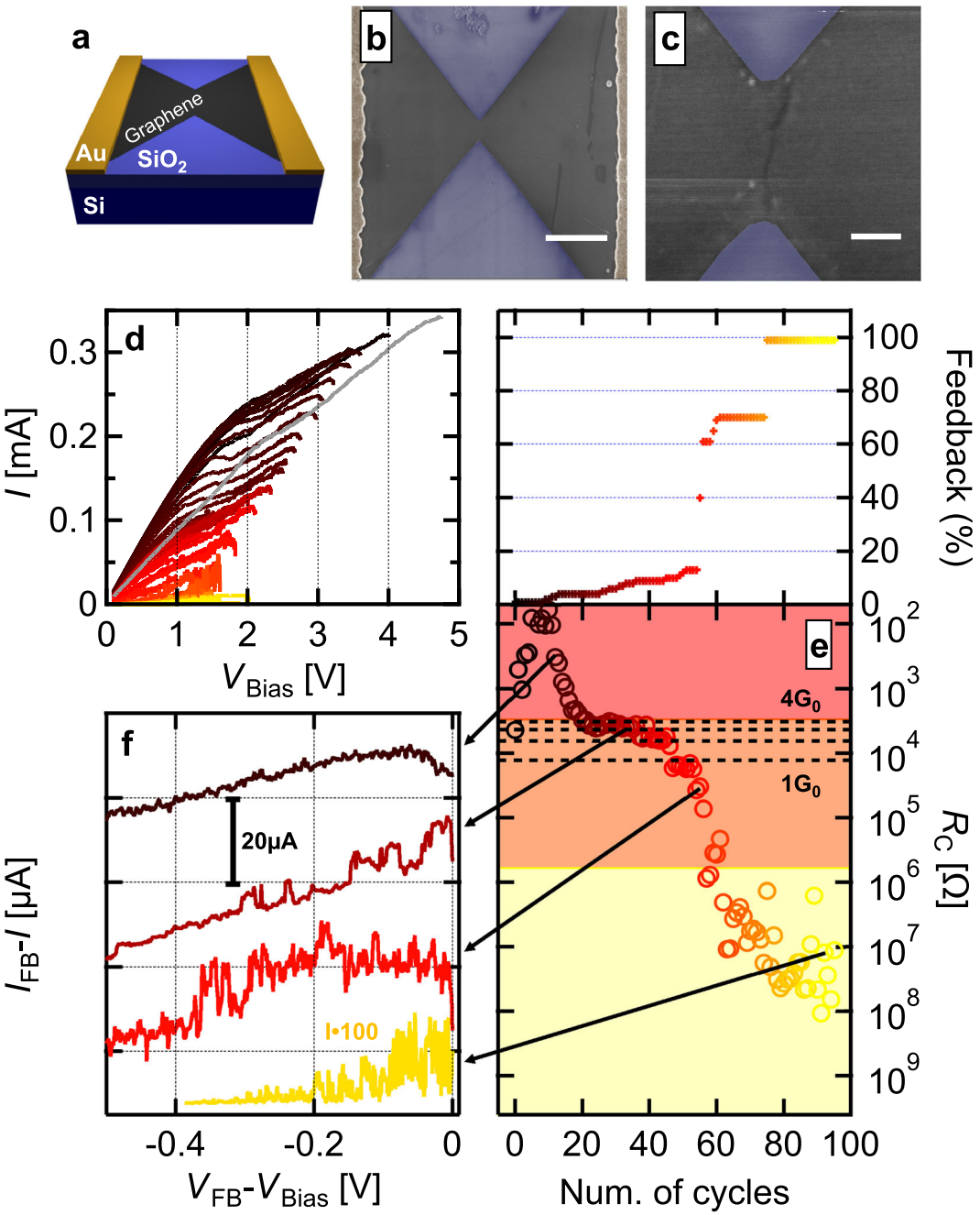

Fig. 1 Gradual, feedback-controlled electrical breakdown of the graphene junctions. a Schematic of our graphene devices. The width of the as-prepared graphene junction at the minimal cross-section is 200 nm. **b** SEM image of the as-prepared bow-tie shaped graphene sheet (gray) terminated by two metal electrodes (yellow). The scale bar indicates 500 nm. **c** Magnified view of the broken graphene nanoconstriction. The nanogap across the graphene sheet is visible as a thin dark gray line at the center. The scale bar indicates 100 nm. **d** Current–voltage traces recorded during the controlled electrobreakdown of a graphene constriction at ambient conditions. The kink around 2.3 V on the first trace (gray) is a characteristic feature arising from the surface cleaning of graphene. **e** Evolution of the low-bias constriction resistance (R_C) as a function of the feedback cycle number for the device shown in **d** using the same color coding. Each data point corresponds to the resistance evaluated at low voltage, i.e., in the linear regime of the actual current–voltage trace. The top panel shows the dynamically changed feedback percentage during the EB process. Note, that only those cycles are displayed, where at least a 200 mV voltage increase was achieved before the feedback event. In the opposite case (i.e., when the relative current decreases compared to the maximal current reaches the threshold feedback percentage within less than 200 mV from zero bias) we automatically consider a false feedback event and elevate the threshold feedback percentage. **f** Four representative EB current–voltage curves magnified around the feedback events. The current values corresponding to the highest resistance (yellow trace) are multiplied by a factor of 100.

during the EB procedure. Typically the lowest resistance does not belong to the first cycle due to the current annealing of the graphene sheet[22] (see Supplementary Note 2 for more details on this phenomenon). Surprisingly, after a well controllable gradual narrowing period, the constriction resistance exhibits a plateau in the regime of the $G_0 = 2e^2/h$ conductance quantum unit. We claim that this plateau is not a conductance quantization feature, rather the resistance noise of the junction rapidly increases and triggers

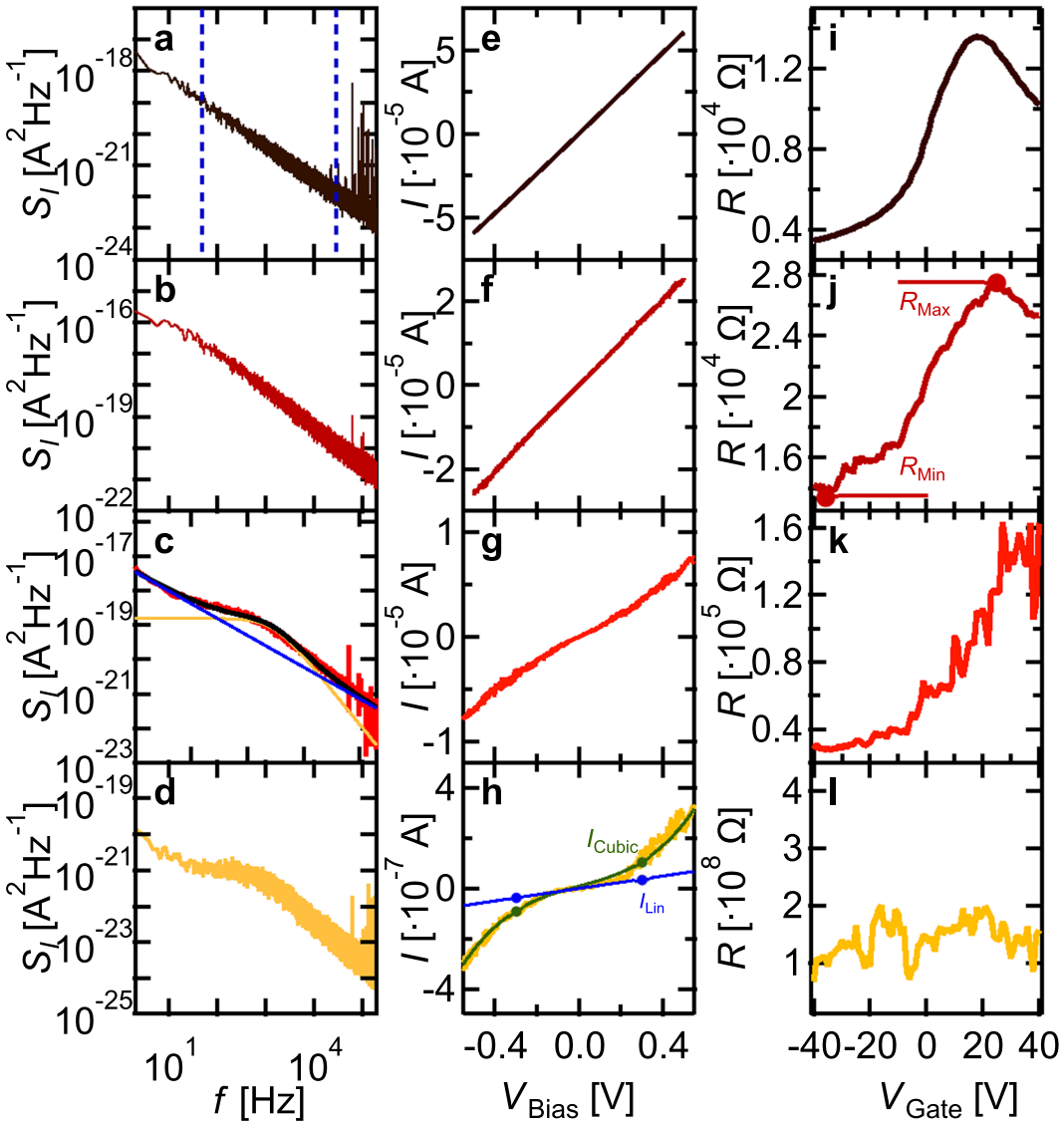

Fig. 2 Representative noise spectra, current-voltage characteristics and gate response curves at different stages of the electrical breakdown. a, **b**, **c**, **d** Power spectral density (PSD) plots, **e**, **f**, **g**, **h** *I*(*V*) and **i**, **j**, **k**, **l** gate response characteristics of graphene bow-tie devices in their initial state (≈8 kΩ, brown curves in **a**, **e**, **i**), in an early stage of the EB (≈20 kΩ, dark red curves in **b**, **f**, **j**), in the narrow nanojunction regime (≈40 − 60 kΩ, red curves in panels **c**, **g**, **k**) and in the tunneling regime (≈50−150 MΩ, yellow curves in **d**, **h**, **l**). The blue dashed lines in **a** illustrate the frequency band of our further analysis (see text). In **c** the fitted 1/*f*-type (blue line), Lorentzian (yellow), and total (black) noise contributions are illustrated (see text). The green and blue lines in **h** respectively illustrate the fitted cubic and linear contributions to the *I*(*V*) curve, from which the degree of the *I*(*V*) nonlinearity is evaluated at 300 mV (see dots, and the detailed description in the text). In **j** the maximum (R_{Max}) and minimum (R_{Min}) resistance is marked in the ±40 V gate voltage window, which are used for the calculation of the relative gate response amplitude (see text). Throughout our analysis, the noise spectra and the *I*(*V*) curves are measured at zero gate voltage.

false feedback events as the quantum conductance is approached and surpassed. Indeed, the magnified final sections of representative voltage ramp cycles demonstrate the significant noise increase (see the dark red, red and yellow curves compared to the brown trace in Fig. 1f). Accordingly, the threshold feedback percentage needs to be significantly increased to proceed with the electrical breakdown (see Fig. 1e top panel).

Noise characteristics of graphene nanojunctions and nanogaps

The elevated noise levels demonstrated in Fig. 1f are consistent with prior studies reporting high current fluctuations as the width of the graphene constriction is reduced below 100 nm.[26–28] Significant noise levels are further maintained in graphene tunnel junctions[29] which was attributed to tunnel barrier-height fluctuations in the nanogap region. In the following, we study this noise enhancement in detail with the goal of understanding the underlying noise generating atomic processes. Thereby we aim at proposing an optimized protocol for the electrical breakdown. First, (i) we perform noise measurements on a statistically relevant number of junctions to map the general evolution of the Δ*I*/*I* relative current fluctuations as the constriction resistance is increased along the EB steps. Next, (ii) we resolve the increasingly dominant single atomic fluctuators along the EB process by decomposing the noise spectra to the 1/*f*-type background of many fluctuators and the Lorentzian contribution arising from single nearby fluctuators. In addition, (iii) we identify the distinct, well separable regimes of the EB process by also evaluating the gate response and *I*(*V*) nonlinearity. Afterward, (iv) we quantitatively analyze the noise evolution in terms of simple models taking into account single-atomic junction-width fluctuations in the

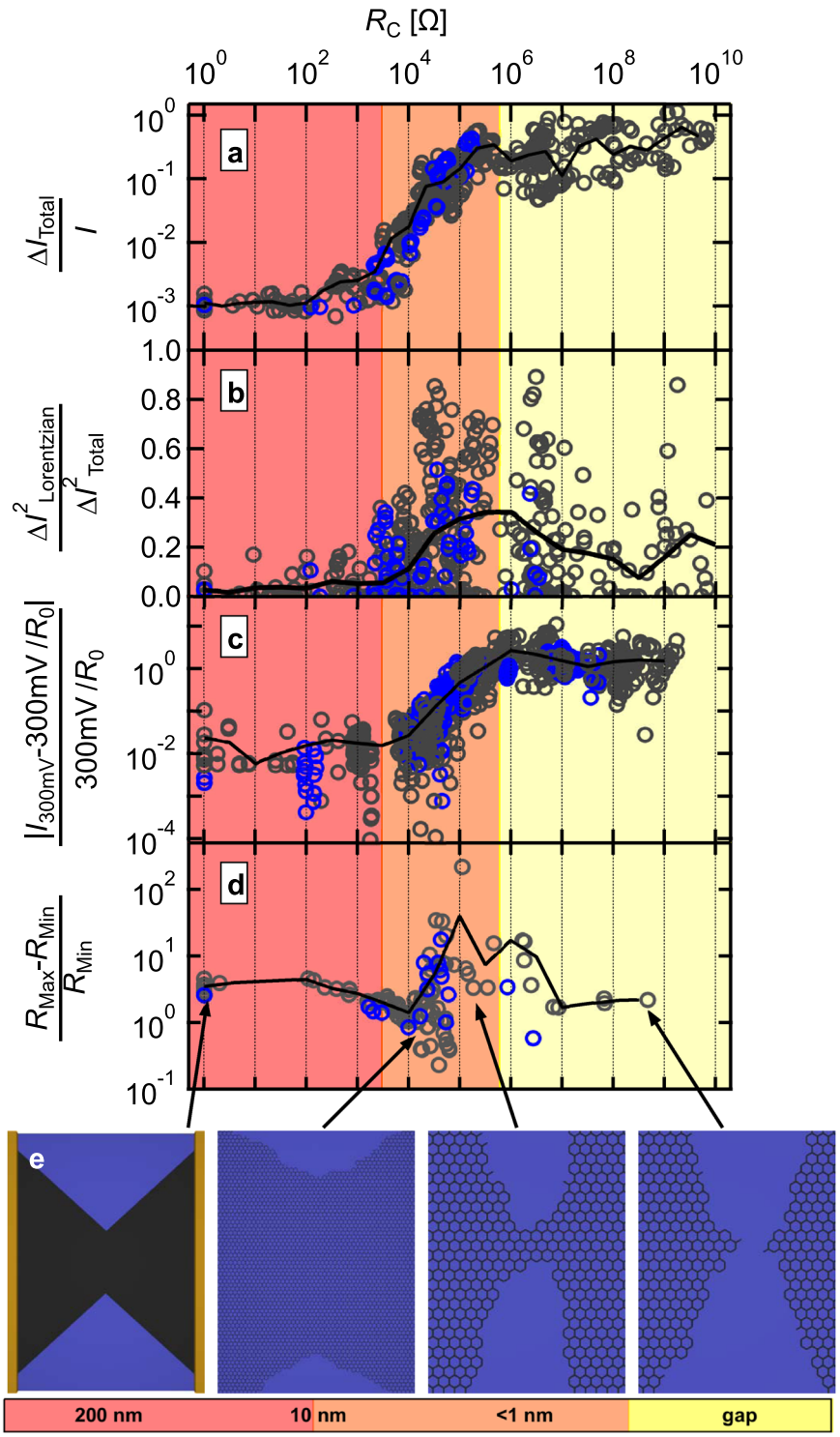

Fig. 3 Resistance dependence of the noise, *I*(*V*) nonlinearity, and gate response characteristics for a statistical ensemble of junctions. The relative current fluctuation (**a**), the relative Lorentzian noise contribution (**b**), the *I*(*V*) nonlinearity (**c**) and the relative gate response amplitude (**d**) as a function of the constriction resistance (R_C) along several steps of the EB process. **a**, **b** [(**c**, **d**)] display data acquired on 10 [6] different devices. The gray (blue) dots correspond to graphene samples patterned on Si/SiO_2 (Si/Si_3N_4) substrates, respectively. The black lines is **a**–**d** represent averaged characteristics. The bottom cartoons (**e**) illustrate the characteristic width of the graphene constriction at the different stages of the breakdown process (see text).

nanometer-sized junction regime, and subatomic gap-size fluctuations in the nanogap regime. Finally, (v) we apply nonlinear noise spectroscopy on the nanogap regime to underpin our gap-size modulation model and to exclude the barrier-height fluctuation model.

To gain a comprehensive electrical characterization of the junction evolution along the EB protocol we regularly stop the EB process to record the S_I current noise power spectral density (Fig. 2a–d), the current–voltage characteristics (Fig. 2e–h) and the gate response characteristics (Fig. 2i–l) of the actual junction (see

Supplementary Note 3 for more details on the noise measurement protocol). We have analyzed a statistical ensemble of EB processes. During each process we have recorded the above characteristics at ≈10 distinct constriction resistance values.

We found that the noise spectra either follow a clear 1/*f*-type frequency dependence (see Fig. 2a, b), or a kink is superimposed on the overall 1/*f*-type background (see Fig. 2c, d). We attribute the emergence of such kinks to a single dominant atomic fluctuator located in the junction region,[30] while an ensemble of remote fluctuators result in the more generic 1/*f*-type background.[31] A single fluctuator with a well-defined τ time constant yields to a Lorentzian-type noise spectrum which is constant at low frequency and follows a $1/f^2$ dependence at $f \gg \tau^{-1}$. In contrast, the Lorentzian spectra of an ensemble of remote fluctuators sum up to a 1/*f*-type envelope. Accordingly, we fit all noise spectra with the

$$S_I(f) = \beta \cdot (f/f_0)^{\gamma} + \frac{\alpha\tau}{1 + (2\pi f\tau)^2} \quad (1)$$

formula, where f_0=1 Hz is the reference frequency, β is the magnitude and $\gamma \approx -1$ is the exponent of the 1/*f*-type noise, α is the low-frequency amplitude of the Lorentzian noise and τ is its time constant. Figure 2c exemplifies the fitted 1/*f*-type (blue) and Lorentzian (yellow) noise contributions together with their superposition (black line). From the fitted spectra we calculate the integrated mean squared current deviation, $(\Delta I_{\mathrm{Total}})^2 = \int S_I(f)df$ for the 50 Hz–30 kHz frequency band (see the blue lines in Fig. 2a), from which the relative $\Delta I_{\mathrm{Total}}/I$ current fluctuation is obtained. Alternatively, we can integrate the $(\Delta I_{\mathrm{Lorentzian}})^2$ mean squared current deviation arising from the Lorentzian noise contribution, and quantify the relative noise contribution of the single dominant fluctuator as $(\Delta I_{\mathrm{Lorentzian}})^2/(\Delta I_{\mathrm{Total}})^2$.

The *I*(*V*) curves are well fitted with an $I_{\mathrm{Cubic}} = I_{\mathrm{Lin}} + b \cdot V^3$ cubic function, where $I_{\mathrm{Lin}} = R_{\mathrm{Lin}} \cdot V$ is the linear part of the *I*(*V*) curve as determined by its low-bias slope, R_{Lin}. We measure the degree of nonlinearity with $(I_{\mathrm{Cubic}} - I_{\mathrm{Lin}})/I_{\mathrm{Lin}}$, which we evaluate at $V_{\mathrm{Bias}} =$ 300 mV (see Fig. 2h). The gate response curves measured in the $V_{\mathrm{Gate}} = \pm 40$ V gate voltage window are characterized by their $(R_{\mathrm{Max}} - R_{\mathrm{Min}})/R_{\mathrm{Min}}$ values (see Fig. 2j).

Figure 3 shows the evolution of the four, above defined characteristic quantities, the relative current fluctuation (a), the relative Lorentzian noise contribution (b), the current–voltage non-linearity (c) and the relative gate response amplitude (d) as a function of the constriction resistance. The statistics are created from the electroburning of 9 graphene nanocontacts fabricated on SiO_2 substrates (gray symbols) and an identical control device utilizing a Si_3N_4 substrate (blue symbols). The evolution of these four characteristic quantities highlights three clearly separated regimes that are established during the EB procedure.

In the first, low resistance regime ($R_C < 3 \cdot 10^3\,\Omega$, red background) the relative current fluctuation remains at its low initial value of 10^{-3} (Fig. 3a), whereas the Lorentzian type noise has negligible contribution (Fig. 3b). The current–voltage traces show ohmic behavior with negligible nonlinearity (Fig. 3c). The relative gate response amplitudes have decreasing tendency, which can be attributed to the shift of the gate response curves to higher resistance, while $R_{\mathrm{Max}} - R_{\mathrm{Min}}$ together with the overall shape of the gate response curve remains roughly unchanged (see the individual curves in Fig. 2i, j). Afterward, at the same resistance regime where the electrical breakdown becomes less controllable ($3 \cdot 10^3\,\Omega < R_C < 6 \cdot 10^5\,\Omega$, orange background) the total current noise rapidly increases by more than two orders of magnitude. Meanwhile, the ratio of the Lorentzian noise significantly enhances, in many junctions it exceeds 50%. In accordance with the noise measurements, both the *I*(*V*) non-linearity and the relative gate response amplitude increase more than two orders of magnitude. Finally, in the high resistance regime ($R_C > 6 \cdot 10^5\,\Omega$, yellow background) the relative current fluctuation remains at high saturated level ($\Delta I/I \approx 0.1-1$) exhibiting high device to device variation. The Lorentzian noise reduces in average, but it still has considerable contribution (see the black line for the mean Lorentzian contribution in Fig. 3b). The *I*(*V*) traces show a saturated nonlinearity, while the relative gate response amplitude decreases to a level, which is consistent with the overall resistance noise in the yellow regime. Regardless of the substrate material all graphene samples show the same features during the electrical characterizations (gray and blue points). This finding demonstrates that the substrate has a significant effect neither on the breakdown process[24] nor on the electrical noise.[26]

We emphasize, that the adequate knowledge of the general noise evolution along the EB cycles allows the optimization of the EB protocol: by consequently setting the threshold feedback percentage according to the average noise level at the actual junction resistance, false or uncontrolled feedback events can be efficiently eliminated. This adaptive control of the electrical breakdown process is demonstrated in Supplementary Note 4.

Before interpreting the above resistance regimes we estimate the relevant length scales in the system. To this end, we analyze the gate response curve in Fig. 2i, which was measured after the current annealing, but the junction was still wide enough to estimate the $\lambda_F \approx 30$ nm Fermi wavelength and the $l \approx 31$ nm mean free path according to common bulk considerations (see Supplementary Note 5 for more details). As the junction narrows toward the mesoscopic regime bulk quantities like conductivity and mobility fail to describe the system. Instead, the resistance of each junction configuration becomes sensitive to the position of individual scattering centers as well as the fine details of quantum interference phenomena[27,32] and edge termination features.[33–35] Our samples are considered as disordered junctions, where neither the condition for ballistic transport nor the presence of a well-defined edge-termination is satisfied, i.e., the conductances are hardly described by simple theoretical considerations. Instead, we estimate the width of our junctions relying on transmission and scanning electron microscopy measurements[34,36,37] delivering empirical relations between the measured junction width and conductance values. These studies have shown that the resistance of graphene nanojunctions increases inversely proportionally to the junction width all the way from the 100 nm scale to contacts with 1−2 nm width. Consequently, the constriction resistance during the whole narrowing process can be approximated as $R_C = \rho \cdot W^{-1}$, where $\rho \approx 172\,\mathrm{k\Omega} \cdot \mathrm{nm}$ is an empirical constant for short single-layer graphene junctions[36] similar to our structures, and *W* is the width in nanometers. Based on this formula, we estimate a constriction width of $W \approx 57$ nm at the border between the red and orange regimes, whereas $W \approx 0.29$ nm is estimated at the border between the orange and yellow regimes. Note, that the latter number is beyond the range of the transmission electron microscopy measurements, i.e., it is considered as a rough estimate reflecting subnanometer-sized, atomic-scale junctions.

Based on these considerations, we argue that the crossover between the red and orange regimes occurs where atomic-scale junction width fluctuations start to dominate over the noise generated in the leads. Along the orange regime, the graphene junction narrows toward the ultimate atomic width, which is reflected in the rapid increase of the relative current fluctuations. Finally, around the border between the orange and yellow regimes the atomic-scale graphene junction breaks, and a tunneling nanogap forms. In the latter (yellow) regime the noise is either related to gap-size variations or barrier height fluctuations. The corresponding states of the junction evolution are illustrated in Fig. 3e.

We argue that electronically transparent, short graphene junctions are only available up to the quantum resistance, $G_0^{-1} \approx 12.9\mathrm{k\Omega}$, which is related to a ≈13 nm wide junction according to the above width estimate formula. At higher resistances, the junctions start to act as barriers, which leads to

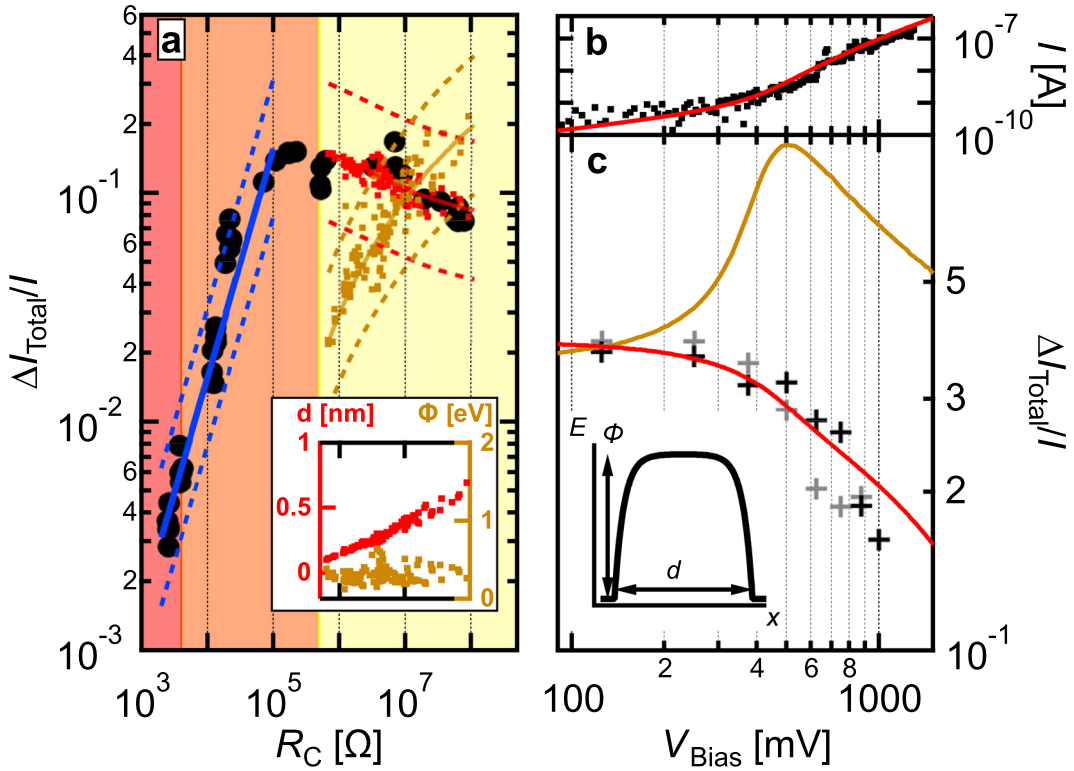

Fig. 4 Model analysis of single-device noise characteristics. a Relative current fluctuation as a function of the constriction resistance (R_C) recorded during the EB process of a specific graphene bow-tie device (black dots). The blue line shows the best fit to the data in the orange nanojunction regime assuming width (W) fluctuations. The dashed lines represent doubled/halved ΔW fluctuations compared to the best-fitting value of $\Delta W = 0.27$ nm. The red and brown dots represent the best fit to the data in the yellow nanogap regime considering purely d or purely Φ fluctuations, and relying on the actual d and Φ values obtained from the Simmons fitting for each junction. The brown and red lines represent the best fitting resistance dependence of $\Delta I/I$ relying on the averaged $\overline{\Phi} = 0.31$ eV barrier height for all junctions. The red and brown dashed lines refer to the calculated noise levels using a doubled/halved $\Delta\Phi$ and Δd fluctuations compared to these best-fitting curves. The inset shows the fitted tunnel barrier heights (brown) and lengths (red) as a function of the resistance. **b** Current–voltage characteristic of a graphene nanogap junction (black dots) and it is fitting by the numerically evaluated Simmons model (red line). **c** Relative current fluctuation as a function of the bias voltage measured right after the $I(V)$ measurement on **b**. The black and gray crosses respectively correspond to the upward and the subsequent downward voltage sweep demonstrating the stability of the junction along the entire 32 s length of the voltage-dependent noise measurement. $\Delta I/I$ starts to decrease at the bias close to the barrier height ($\Phi = 0.35$ eV). The red and brown lines represent the calculated voltage dependence of the relative current fluctuation relying on purely d and Φ fluctuations, respectively. The inset shows the schematic of the potential barrier used for the numerical evaluation of the Simmons model.

the emergence of nonlinear features in the $I(V)$ curve. Furthermore, depending on the actual junction arrangement, resonant transport features may also arise in the gate response.[26,32] Note, that whereas the relative current fluctuations and the relative Lorentzian contributions already start to increase in the $k\Omega$ regime (see Fig. 3a, b), pronounced $I(V)$ nonlinearity and intense gate response are hallmarks of the $R_C > G_0^{-1}$ resistance regime (Fig. 3c, d).

Model analysis of the noise characteristics

To validate our intuitive conceptions about the dominant noise sources, we turn to the model analysis of the above scenarios. For this purpose we quantitatively analyze the tendencies of the relative current fluctuations for a particular device (see black dots in Fig. 4a).

First, we focus on the orange nanojunction regime. Considering ρ and W fluctuations in the above empirical resistance estimate formula, the relative current fluctuation is expressed as $(\Delta I/I)^2 = (\Delta W \cdot R_C/\rho)^2 + (\Delta\rho/\rho)^2$. The second term is independent of the width, and therefore it can only contribute to the baseline of the noise level ($\approx 10^{-3}$). Therefore, in the orange regime, we attribute the noise increase to the first term which implies a straight line with a unity slope on the $\log(\Delta I/I) - \log(R_C)$ plot, whose intercept corresponds to $\Delta W/\rho$. By fitting a straight line to our data (see the blue line in Fig. 4a) we obtain a width fluctuation of $\Delta W = 0.27$ nm. The dashed blue lines demonstrate the calculated noise level using a doubled/halved ΔW fluctuation. This analysis confirms that the effective width of the junction fluctuates on the scale of the lattice constant. This atomic-scale junction-width fluctuation accounts for the observed two orders of magnitude increase of the relative noise as the junction width decreases from a few tens of nanometers to the atomic regime. The picture of atomic-scale fluctuations is also supported by the dominance of the Lorentzian contribution, i.e., the dominance of single fluctuators in the spectrum (Fig. 3b). We note, that this effective width fluctuation is not necessarily related to the direct width-fluctuation of the graphene lattice, but further features, like edge termination fluctuations[38] or charge trapping/de-trapping at the disordered graphene edges[26,39] may also yield an effective width fluctuation.

Next, we analyze the resistance dependence of $\Delta I/I$ in the yellow, nanogap regime. Prior studies have shown[13,21,22,24,29,32] that the transport through graphene nanogaps is well described by the Simmons model[40] relying on two key parameters, the Φ height and the d length of the tunneling barrier between the two sides of the nanogap. Here, we also describe the $I(V)$ characteristics in terms of a numerically evaluated Simmons model (see Supplementary Note 6) considering a rounded rectangular

potential barrier (see inset of Fig. 4c). The rounded barrier ensures the smooth transition from the direct tunneling to the field electron emission regime, which is essential in our later analysis of nonlinear noise phenomena. We measure the $I(V)$ characteristic after each EB step in the yellow resistance regime and determine the d and Φ parameters by Simmons fitting (see inset of Fig. 4a). This analysis reveals that Φ remains roughly constant ($\overline{\Phi} = 0.31 \pm 0.1$ eV) in the entire yellow regime, while the increase of the d barrier length is proportional to the logarithm of the resistance.

We emphasize, that in the framework of the Simmons model, a completely different resistance dependence of $\Delta I/I$ is obtained if solely barrier-length fluctuations or solely barrier-height fluctuations are considered as the dominant noise source (see Supplementary Note 6). This is demonstrated by the red (brown) dots in Fig. 4a, where $\Delta I/I$ is calculated by inserting the fitted d and Φ values of the actual junction to the Simmons model, and considering a constant Δd gap-size fluctuation (red) or a constant $\Delta\Phi$ barrier-height fluctuation (brown) within the entire yellow regime. The plotted red (brown) dots represent the $\Delta d = 0.012$ nm ($\Delta\Phi = 0.042$ eV) values, for which the calculated resistance dependence fits the measured resistance dependence of $\Delta I/I$ the best. The barrier-height fluctuation model yields a comparable relative fluctuation ($\Delta\Phi/\Phi \approx 0.13$) as a previously applied tight-binding model[29] ($\Delta\Phi/\Phi \approx 0.057$). The latter model successfully accounted for the observed temperature and frequency dependence of the noise in graphene nanogaps, however, our analysis demonstrates that the measured *resistance dependence* of $\Delta I/I$ is completely inconsistent with the barrier-height fluctuation model (brown dots). In contrast, a 10 pm scale gap-size fluctuation (red dots) i.e., subatomic fluctuations of the graphene nanogap edges well describe the observed resistance dependence of the relative current fluctuations.

Finally, we apply nonlinear noise spectroscopy to further support the clear dominance of gap-size fluctuations over barrier-height fluctuations in the noise characteristics of graphene nanogaps. So far all presented noise measurements were restricted to sufficiently low voltage driving, where the linearity of the $I(V)$ curve is satisfied. In this linear regime the relative resistance and current noise values are equal, $\Delta R/R = \Delta I/I$, i.e., steady-state resistance fluctuations yield voltage-independent $\Delta I/I$ values. However, in the nonlinear transport regime $\Delta I/I$ also exhibits a distinct voltage dependence. Furthermore, the nonlinearity of the $I(V)$ curve converts to a completely different voltage dependence of $\Delta I/I$, when purely gap-size fluctuations or purely barrier-height fluctuations are considered.

Figure 4c shows the voltage dependence of $\Delta I/I$ for a representative nanogap junction (see the black/gray crosses corresponding to the upward/downward voltage sweep), whereas the $I(V)$ curve of the same junction is shown in Fig. 4b (black dots). From the latter, the Simmons fitting (red curve) reveals the barrier parameters ($\Phi = 0.35$ eV, $d = 0.91$ nm). Using these parameters we determine the amplitude of pure gap-size fluctuations ($\Delta d = 0.054$ nm) and pure barrier-height fluctuations ($\Delta\Phi = 0.057$ eV) in such a way that the relative current fluctuations calculated from the Simmons model reproduce the measured constant low-bias $\Delta I/I$ values. The measured noise data demonstrate, that the voltage independence of $\Delta I/I$ holds up to 300 mV. At higher voltage, the relative current fluctuations markedly decrease with the voltage. Consistent with our previous findings, the gap-size fluctuation model (red line) reproduces the measured noise dependence. In sharp contrast, the barrier-height fluctuation model (brown curve) is fully inconsistent with the measured noise data. In this case, the calculated voltage dependence of $\Delta I/I$ exhibits a peak in the voltage regime corresponding to the barrier height. At this bias voltage, the profile of the potential barrier changes from trapezoidal to triangular and the current becomes more sensitive to barrier height fluctuations.

In the above analysis the $d = 0.91$ nm length of the tunneling barrier is considered as an effective gap size. Due to the exponential dependence of the current on the length of the barrier we anticipate that this effective length is close to the actual size of the nanogap at the narrowest spot, and the ≈30% Lorentzian contribution to the noise (Fig. 3b) is related to a single fluctuator near the narrowest spot. However, the electrical breakdown is considered as a self-limiting process, i.e., once a segment is disconnected, it does not widen further. This means, that the gap length remains in the range of the few nanometers along the entire width of the graphene stripe.[22] Accordingly, it is conceivable that further segments of the nanogap also contribute to the current, and the fluctuators around these segments contribute to the 1/*f*-type background noise. The latter background noise may also relate to the diffusion of adatoms around the narrowest spot lacking a well-defined time-scale, similarly to the sub-Ångström gap-size fluctuations in atomic-sized gold tunnel junctions.[41] In contrast, the thermal bond fluctuations according to the Bose-Einstein distribution of the phonon modes are not considered as a source of the 1/*f*-type background noise. The latter considerations are discussed further in Supporting Note 6.

Conclusions

In conclusion, we have demonstrated that the advanced analysis of low-frequency noise measurements supplies a rich source of information on the controlled electrobreakdown process of graphene nanojunctions. Following the evolution of the relative noise amplitudes we were able to optimize the electrical breakdown protocol and to identify distinct regimes of the nanogap formation process. The latter clearly highlighted the crossover between unbroken atomic-scale junctions and nanogap devices. Analyzing the frequency dependence of the noise, we are able to follow how single atomic fluctuators start to dominate over a broader 1/*f*-type noise background as the ultimate atomic junction dimensions are approached. The numerical analysis of the markedly different resistance dependence of the noise in the nanojunction and nanogap regimes allowed us to identify the microscopic noise generating mechanisms. In the former case atomic-scale junction-width fluctuations, whereas in the latter subatomic gap-size fluctuations are identified as the major noise sources. Finally, we applied the approach of nonlinear noise spectroscopy demonstrating that the conversion of current–voltage nonlinearity to nonlinear noise phenomena is sensitive to the microscopic origin of the dominating fluctuations. Using this distinction we provided an unambiguous proof that gap-size fluctuations are highly dominating over barrier-height fluctuations in graphene nanogap devices. According to pioneering results on MoS_2 nanojunctions[42,43] and the study of the electrical breakdown in MoS_2 field-effect transistors[44] we believe that the presented adaptive breakdown protocol and the scheme of the noise measurements are well applicable in other sufficiently conducting 2D materials as well.

METHODS

Sample fabrication

The large area single-layer graphene is prepared on 25 μm thick copper foil in a low-pressure CVD furnace following the protocol in ref. [25]. Before loading the copper into the CVD chamber it is cleaned with acetic acid and rinsed in DI water and ethanol. During the deposition the furnace is kept at 1000 °C besides 200 sccm argon, 20 sccm hydrogen and 0.1 sccm CH_4 gas flow for 50 min. The graphene is placed onto the doped Si substrate by wet transfer method, using 0.1 M solution of ammonium persulfate for copper etching and DI water to rinse the graphene. The Ti/Au electrodes are patterned using electron beam lithography and metal evaporation, whereas the graphene sheet is tailored into notched ribbons by using a second electron beam lithography process and oxygen plasma etching.

Noise measurement

The noise measurements are performed by recording the temporal current fluctuation using the dedicated setup schematically shown in Supplementary Fig. 3a. The circuit is driven by an Agilent 33220A arbitrary waveform generator, whereas the current is amplified by a Femto DLPCA-200 low-noise current amplifier and acquired by a NI PCI-5922 digitizer card with a built-in antialiasing filter. To suppress the voltage noise arising from the function generator a low-pass filter with 0.26 Hz cut-off frequency is used. The current noise power density spectra are calculated by using the built-in FFT function of the IgorPro 8 software. The further experimental details of the noise measurements are available in Supplementary Note 3.

Numerical fitting of *I*(*V*) characteristics

In the nanogap regime the measured *I*(*V*) characteristics are fitted against numerically evaluated Simmons model using the least root-mean-square deviation method. The details on the fitting of the resistance-dependent noise data and the nonlinear noise spectra in the nanogap regime are available in Supplementary Note 6.

DATA AVAILABILITY

The datasets generated during and/or analyzed during the current study are available from the corresponding author (A.H.) on reasonable request.

CODE AVAILABILITY

The codes that support the findings of this study are available from the corresponding author (A.H.) on reasonable request.

Received: 26 November 2020; Accepted: 23 April 2021;
Published online: 26 May 2021

REFERENCES

1. An analogue future for 2D. *Nat. Electron.* **3**, 437–437 (2020).
2. Akinwande, D., Petrone, N. & Hone, J. Two-dimensional flexible nanoelectronics. *Nat. Commun.* **5**, 5678 (2014).
3. Akinwande, D. et al. Graphene and two-dimensional materials for silicon technology. *Nature* **573**, 507–518 (2019).
4. Kim, M. et al. Zero-static power radio-frequency switches based on MoS_2 atomristors. *Nat. Commun.* **9**, 2524 (2018).
5. Kim, M. et al. Analogue switches made from boron nitride monolayers for application in 5G and terahertz communication systems. *Nat. Electron.* **3**, 479–485 (2020).
6. Bourzac, K. Electronics: back to analogue. *Nature* **483**, S34–S36 (2012).
7. Polyushkin, D. K. et al. Analogue two-dimensional semiconductor electronics. *Nat. Electron.* **3**, 486–491 (2020).
8. Polat, E. O. et al. Flexible graphene photodetectors for wearable fitness monitoring. *Sci. Adv.* **5**, eaaw7846 (2019).
9. Goossens, S. et al. Broadband image sensor array based on graphene–CMOS integration. *Nat. Photon.* **11**, 366–371 (2017).
10. Pan, C. et al. Reconfigurable logic and neuromorphic circuits based on electrically tunable two-dimensional homojunctions. *Nat. Electron.* **3**, 383–390 (2020).
11. Manzeli, S., Ovchinnikov, D., Pasquier, D., Yazyev, O. V. & Kis, A. 2D transition metal dichalcogenides. *Nat. Rev. Mater.* **2**, 17033 (2017).
12. El Abbassi, M. et al. Robust graphene-based molecular devices. *Nat. Nanotechnol.* **14**, 957–961 (2019).
13. Xu, Q. et al. Single electron transistor with single aromatic ring molecule covalently connected to graphene nanogaps. *Nano Lett.* **17**, 5335–5341 (2017).
14. Mol, J. A. et al. Graphene-porphyrin single-molecule transistors. *Nanoscale* **7**, 13181–13185 (2015).
15. Lau, C. S. et al. Redox-dependent Franck-Condon blockade and avalanche transport in a graphene-fullerene single-molecule transistor. *Nano Lett.* **16**, 170–176 (2016).
16. Heerema, S. J. & Dekker, C. Graphene nanodevices for DNA sequencing. *Nat. Nanotechnol.* **11**, 127–136 (2016).
17. Puczkarski, P., Swett, J. L. & Mol, J. A. Graphene nanoelectrodes for biomolecular sensing. *J. Mater. Res.* **32**, 3002–3010 (2017).
18. Behnam, A. et al. Nanoscale phase change memory with graphene ribbon electrodes. *Appl. Phys. Lett.* **107**, 123508 (2015).
19. Pósa, L. et al. Multiple physical time scales and dead time rule in few-nanometers sized graphene-SiO_x-graphene memristors. *Nano Lett.* **17**, 6783–6789 (2017).
20. Sarwat, S. G. et al. Scaling limits of graphene nanoelectrodes. *Nano Lett.* **17**, 3688–3693 (2017).
21. Prins, F. et al. Room-temperature gating of molecular junctions using few-layer graphene nanogap electrodes. *Nano Lett.* **11**, 4607–4611 (2011).
22. Nef, C. et al. High-yield fabrication of nm-size gaps in monolayer CVD graphene. *Nanoscale* **6**, 7249–7254 (2014).
23. Lau, C. S., Mol, J. A., Warner, J. H. & Briggs, G. A. D. Nanoscale control of graphene electrodes. *Phys. Chem. Chem. Phys.* **16**, 20398–20401 (2014).
24. El Abbassi, M. et al. From electroburning to sublimation: substrate and environmental effects in the electrical breakdown process of monolayer graphene. *Nanoscale* **9**, 17312–17317 (2017).
25. Thodkar, K. et al. Restoring the electrical properties of CVD graphene via physisorption of molecular adsorbates. *ACS Appl. Mater. Interfaces* **9**, 25014–25022 (2017).
26. Fried, J. P. et al. Large amplitude charge noise and random telegraph fluctuations in room-temperature graphene single-electron transistors. *Nanoscale* **12**, 871–876 (2020).
27. Sadeghi, H. et al. Conductance enlargement in picoscale electroburnt graphene nanojunctions. *Proc. Natl. Acad. Sci. USA* **112**, 2658–2663 (2015).
28. Xu, G. et al. Enhanced conductance fluctuation by quantum confinement effect in graphene nanoribbons. *Nano Lett.* **10**, 4590–4594 (2010).
29. Puczkarski, P. et al. Low-frequency noise in graphene tunnel junctions. *ACS Nano* **12**, 9451–9460 (2018).
30. Sánta, B. et al. Noise tailoring in memristive filaments. *ACS Appl. Mater. Interfaces* **13**, 7453–7460 (2021).
31. Balandin, A. A. Low-frequency 1/f noise in graphene devices. *Nat. Nanotechnol.* **8**, 549–555 (2013).
32. Gehring, P. et al. Quantum interference in graphene nanoconstrictions. *Nano Lett.* **16**, 4210–4216 (2016).
33. Wurm, J., Wimmer, M. & Richter, K. Symmetries and the conductance of graphene nanoribbons with long-range disorder. *Phys. Rev. B* **85**, 245418 (2012).
34. Han, M. Y., Özyilmaz, B., Zhang, Y. & Kim, P. Energy band-gap engineering of graphene nanoribbons. *Phys. Rev. Lett.* **98**, 206805 (2007).
35. Evaldsson, M., Zozoulenko, I. V., Xu, H. & Heinzel, T. Edge-disorder-induced Anderson localization and conduction gap in graphene nanoribbons. *Phys. Rev. B* **78**, 161407 (2008).
36. Qi, Z. J. et al. Correlating atomic structure and transport in suspended graphene nanoribbons. *Nano Lett.* **14**, 4238–4244 (2014).
37. Wang, Q. et al. Fabrication and in situ transmission electron microscope characterization of free-standing graphene nanoribbon devices. *ACS Nano* **10**, 1475–1480 (2016).
38. Takashima, K. & Yamamoto, T. Conductance fluctuation of edge-disordered graphene nanoribbons: crossover from diffusive transport to Anderson localization. *Appl. Phys. Lett.* **104**, 093105 (2014).
39. Shao, Q. et al. Flicker noise in bilayer graphene transistors. *IEEE Electron Device Lett.* **30**, 288–290 (2009).
40. Simmons, J. G. Generalized formula for the electric tunnel effect between similar electrodes separated by a thin insulating film. *J. Appl. Phys.* **34**, 1793–1803 (1963).
41. Adak, O. et al. Flicker noise as a probe of electronic interaction at metal-single molecule interfaces. *Nano Lett.* **15**, 4143–4149 (2015).
42. Chen, Q. et al. Atomically flat zigzag edges in monolayer MoS_2 by thermal annealing. *Nano Lett.* **17**, 5502–5507 (2017).
43. Wang, K. et al. Electrical control of charged carriers and excitons in atomically thin materials. *Nat. Nanotechnol.* **13**, 128–132 (2018).
44. Lembke, D. & Kis, A. Breakdown of high-performance monolayer MoS_2 transistors. *ACS Nano* **6**, 10070–10075 (2012).

ACKNOWLEDGEMENTS

The research reported in this paper was supported by the BME Nanotechnology and Materials Science TKP2020 IE grant of NKFIH Hungary (BME IE-NAT TKP2020) and the NKFI K119797 grant. The authors are thankful to Prof. M. Calame for sharing expertise on the nanogaps electrical breakdown and for useful discussions and suggestions.

AUTHOR CONTRIBUTIONS

The sample preparation, the development of the gradual feedback-controlled electrobreakdown protocol and the model analysis of the noise data were performed by L. Pósa. The noise measurement system was developed and the noise measurements were performed by Z. Balogh, D. Krisztián, and P. Balázs. The CVD graphene sheets were produced by R. Furrer and transferred to the Si wafers by B. Sánta. The manuscript was written by L. Pósa, A. Halbritter, Z. Balogh, and M. Csontos. The project was supervised by A. Halbritter. All authors contributed to the discussion of the results. L. Pósa and Z. Balogh contributed equally to this work and are considered as co-first authors.

COMPETING INTERESTS

The authors declare that there are no competing interests.

ADDITIONAL INFORMATION

Supplementary information The online version contains supplementary material available at https://doi.org/10.1038/s41699-021-00237-w.

Correspondence and requests for materials should be addressed to A.H.

Reprints and permission information is available at http://www.nature.com/reprints

Publisher's note Springer Nature remains neutral with regard to jurisdictional claims in published maps and institutional affiliations.